Progress in Physics of Applied Materials 6 (2026), Serial Number 13, 273-284

Semnan University

Progress in Physics of Applied Materials

journal homepage: https://ppam.semnan.ac.ir/

Ginger-Extract–Modified ZnO Nanoparticles for Antibacterial Applications

Ahmed H. Ali [*a], Ahlam Ismael Al-Obaidi [b], Ahmed AL-Jumaili [a,c]

[a]*Department of Medical Physics, College of Applied Science, University of Fallujah, 31002 Iraq*
[b]*College of Pharmacy, University of Mashreq, Baghdad, Iraq*
[c]*Electronics Materials Lab, College of Science and Engineering, James Cook University, QLD, 4811 Australia*

ARTICLE INFO

Article history:
Received: 20 December 2025
Revised: 22 February 2026
Accepted: 26 February 2026
Published online: 25 April 2026

Keywords:
Zinc oxide nanoparticles;
Ginger extract;
Green synthesis;
Antibacterial activity;
Optical properties.

ABSTRACT

This study confirmed the green formation of zinc oxide nanoscale particles (ZnO-NPs) via the extract of ginger rhizome as a sustainable and effective stabilizing agent. Surface modification by ginger-derived phytochemicals resulted in a distinct red shift in optical absorption and a narrowing of the bandgap, indicating successful electronic tuning of the material. In comparison to pure ZnO-NPs, the ginger-mediated approach produces much smaller crystallites and a more uniform particle dispersion, according to structural and morphological characterizations. The biological performance of the nanoparticles was directly improved by these physicochemical changes; the modified GE-ZnO-NPs demonstrated greater antibacterial and antibiofilm efficacy against Staphylococcus aureus. This work presents a sustainable method for creating bio-active nanomaterials with improved performance for antimicrobial functions by emphasizing the cooperative role of phytochemical functionalization in fine-tuning particle size and surface chemistry.

1. Introduction

Significant efforts have been made to adapt nanomaterials to the requirements of existing technologies. The effect of quantum size and the high ratio of surface area to volume of nanomaterials make them more reactive and may lead to some interesting physical and chemical properties compared to their bulk ones [1-3]. Nanomaterials' properties make them important and useful in catalytic converters, environmental optoelectronics, and biological applications.

Zinc oxide nanoparticles (ZnO-NPs) are of interest in materials due to their unique structural, electrical, and surface properties [4-7]. When scaled down to the nanoscale, ZnO has been found to possess enhanced surface reactivity and altered electronic properties resulting from quantum confinement and an enlarged specific surface area [8]. Improved photocatalytic effectiveness, antibacterial characteristics, and regulated optical response result from these advancements. ZnO-NPs can disrupt bacterial/mammalian cell membranes, produce ROS, release ions, and change chemically, making them promising antibacterial and therapeutic agents [9].

In some biological situations, ZnO nanoparticles have photochemical limitations (rapid charge-carrier recombination and limited visible-light absorption) and practical disadvantages (photo-corrosion and reduced bactericidal efficiency) [10-13]. Researchers have explored adding natural components such as plant leaf extract, polymers, or metal doping [14, 15]. These changes may increase nanoparticle stability, surface reactivity, biocompatibility, and optical or catalytic properties, improving them for industrial or biological applications [16, 17]. These doped or hybrid ZnO systems outperform pure nanoparticles and demonstrate the possibility of integrating nanoparticles with functional or bioactive additives [18-20].

* Corresponding author.
E-mail address: ahmed.hussein.ali@uofallujah.edu.iq

Cite this article as:

Ali, A.H., Ismael Al-Obaidi, A. and AL-Jumaili, A., 2026. Ginger-Extract–Modified ZnO Nanoparticles for Antibacterial Applications. *Progress in Physics of Applied Materials*, *6*(4), pp.273-284. DOI: **10.22075/ppam.2026.40113.1194**

Many green synthesis methods use generic plant extracts, which lack chemical specificity for nanoparticle optimization. Ginger extract is particularly for its high gingerol and shogaol content, which provide more specialized bioactive than phenolic sources. More experimental effort is required to focus on specific phytochemicals to achieve targeted electronic tuning and enhanced biofilm penetration, addressing a critical gap in the development of high-performance, bio-functionalized ZnO-NPs. Thus, in this work, ZnO-NPs were experimentally manufactured to systematically estimate the effect of Ginger extract (GE-ZnO-NPs) on their structural, optical, and antimicrobial performance. The produced nanostructured ZnO were analytically investigated using FTIR, XRD, SEM, EDX and UV-Vis spectroscopy for measurements of their composition, morphology and optical behavior.

2. Materials and Methods

2.1. Ginger Extraction and Nanostructured ZnO Synthesis

Fresh Zingiber officinale rhizomes were washed, peeled, and finely chopped. 20 g of the rhizome was boiled in 100 mL of deionized water (1:5 w/v ratio) at 80 °C for 30 minutes. The resultant material was then filtered twice using Whatman No. 1 filter paper and reserved at 4 °C. The phytochemical profile primarily consisting of gingerols, shogaols, and polyphenols.

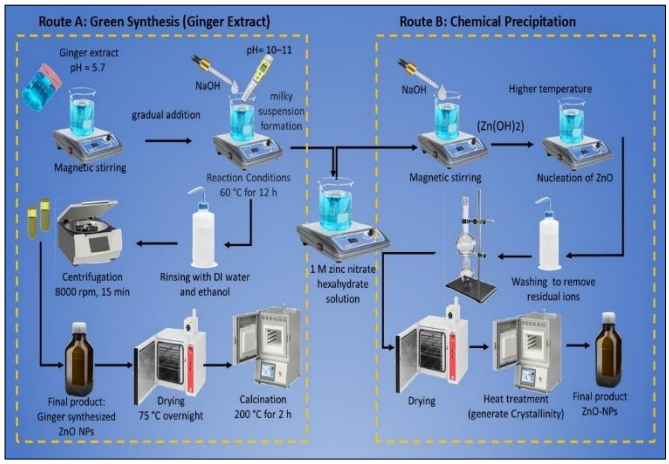

Fig. 1. Schematic figure illustrating the two synthesis routes for zinc oxide nanoparticles (ZnO NPs). Route A (left) shows ginger extract green synthesis, while Route B (right) shows chemical precipitation with higher temperatures and calcination.

Fig. 1 shows the experimental 1 M zinc nitrate hexahydrate Zn $(NO_3)2.6H_2O$ solution prepared by dissolving the appropriate weight in deionized water with magnetic stirring. With constant stirring, ginger extract (pH = 5.7) was slowly added to the zinc precursor solution (1:1, v/v). The milky suspension was formed by gradually adding NaOH solution to the reaction mixture to raise its pH to 10-11. To create zinc particles, the mixture was stirred at 60 °C for 12 hours. After centrifuging at 8000 rpm for 15 minutes, the precipitate was washed with deionized water and ethanol to remove organics and dried at 75 °C for 24 hours. To crystallize dehydrated powder, it was calcined at 200 °C for 2 hours.

Traditional chemical precipitation was used to manufacture ZnO nanoparticles for comparison. Magnetic stirring formed a 1M zinc nitrate hexahydrate suspension in deionized water. Sodium hydroxide and zinc hydroxide intermediates created an alkaline environment, that heated into ZnO. The reaction blend was heated to complete the nucleation and growth of ZnO nanoparticles. The precipitated solid product was collected, washed to remove ions, and dried. The powder was heat-treated to crystallize and phase pure ZnO nanoparticles.

2.2. Characterization Techniques

To evaluate their structural properties, advanced analytical methods were used to study S1 (pure ZnO) and S2 (ZnO-ginger mixture). Sample S1 (pure ZnO chemically precipitated) was used as the control to determine how ginger extract affected nanoparticle characteristics. UV-Vis has been employed as a reliable and direct approach to verify the synthesis of nanoparticles. Spectrophotometry (UV-1900i, UV-Vis) was employed to assess the UV-Vis absorption spectra of the fabricated samples within the range of 190–1100 nm. FTIR spectroscopy analysis is conducted to ascertain the presence of biomolecules in the generated samples. Spectra with a resolution of 3 cm^{-1} and a range of 400 to 4000 cm^{-1} were gathered for a precise and thorough examination. A diffractometer (Bruker AXS SE, USA) with a monochrome source of Cu Kα irradiation was used to conduct the X-ray diffraction (XRD) analysis. The scanning range used to record the diffraction patterns was 7° to 80° (2θ). Scanning field emission electron microscopy device (FESEM, Inspect F50, FEI Company, USA) was employed to thoroughly inspect the ZnO nanoparticles' surface morphology and structural characteristics. The elemental composition was additionally determined by X-ray examination (EDX) with (EDAX, USA). For the antibacterial assays, ginger extract alone and the solvent (deionized water) were used as negative controls to confirm that the enhanced bioactivity was specifically due to the GE-ZnO-NPs and not the residual solvent or extract alone.

All experiments, including the antibacterial and antibiofilm assays, were performed in triplicate (n=3). Statistical significance was determined retaining one-way ANOVA afterward Tukey's post-hoc test for multiple comparisons, with a threshold of $p < 0.05$ set for significance. The numerical data were analyzed in OriginLab (Version 2024).

3. Results and Discussion

3.1. Optical Properties

UV-Vis spectroscopy the optical absorption of the synthesized samples were investigated by UV-vis spectrophotometer depicted in figure 2 (A). The absorption spectrum of S1 showed two weak but well-defined peaks at ~198 nm and ~338 nm, corresponding to native electronic transitions in ZnO molecules. The 198 nm band is caused by charge transfer from O^{2-} to Zn^{2+} ions in the crystal lattice, showing localized electronic excitations of ZnO.

[21]. The 338-nm band corresponds to the direct fundamental transition from one band to the other in wurtzite-type ZnO and is an excitation of electrons (simply from valence bands to conduction bands) [22].

While the presence of peaks and their relatively low intensity in S1 show that stabilizer-free synthesized nanoparticles are not fully crystallized, containing lattice defects and aggregated particles. Such structural defects often generate shallow traps and oxygen vacancies resulting in the development of secondary peak(s) at deep UV range such are observed at 198 nm.

Comparison between absorption spectra of S1 and S2 in shown that two distinct and more intensified absorption peaks at 197 nm and 375 nm were appeared accredited to the influence of ginger extract on optical behavior of nanoparticles. The peak at 197 nm is caused by a deep UV electronic transition in the ZnO lattice. A near band edge transition with defect states and (32.83) (PyObjective (Py)) individuals is observed at 375 nm, with Py7 intensity increasing. The band-edge absorption peak of S2 changed from 338 to 375 nm, indicating ginger phytochemical surface modification and defect-induced electronic states lowering bandgap energy. S1's band edge was less prominent between 198 and 338 nm. Organic molecules modify nanoparticles, causing ginger phytochemicals like phenols, flavonoids, and terpenoids to interact strongly with zinc, causing this red shift. During and after synthesis, these biomolecules donate electrons, permeate flaws, and form organic layers that stabilize nanoparticles and prevent aggregation [21-23].

This interaction induces a slight electronic hybridization of the ZnO orbitals and the organic molecular orbitals, which effectively reduces the conduction and valence bandwidths. Consequently, a red-shift in absorption is observed, as has been reported for other green-synthetic zinc systems using Aloe vera and Neem extracts [24]. The increased absorption of S2 compared to S1 further promotes the formation of highly crystalline and uniformly distributed nanoparticles, which is in line with plant-mediated synthesis, where organic molecules are involved in nucleating and growing particles in narrow size ranges.

Using the Tauc relation for direct bandgap semiconductors, the optical bandgap energies were assessed to be 3.31 eV for S1 and 3.21 eV for S2. The 0.10 eV band gap reduction shows that ginger extract introduces structural defects and oxygen vacancies in the ZnO lattice, structure building and promote a red shift in the absorption edge, increasing near-visible light absorption. Similar phenomena were documented by Aliannezhadi et al. [21], who reported **a** red shift in ginger-mediated ZnO samples due to defect formation and oxygen vacancies.

In addition, the improved peak sharpness and smoothness of the absorption edges of S2 reflect better crystallinity and reduced structural disorder. The ginger biomolecules likely reduced surface stress during growth, resulting in ZnO nanocrystals with well-ordered lattice edges and fewer surface traps. This structural integrity minimizes non-radiative recombination losses and improves optical response, which is in line with the reports from other ZnO systems with green synthetic structures showing increased absorption near the band edge [23, 25].

Spectral properties of S2 also indicate a more pronounced absorption effect at the near-band edge, which can be attributed to increased excitatory transitions and a pooled charge carrier response associated with donor states mediated by defects rather than to any plasmonic behavior. Increased absorption indicates a higher density of electronic states associated with the surface and improved dielectric confinement, reflecting increased electronic coupling and optical sensitivity in a bio- assisted composite structure [21, 22, 26].

The UV–Vis results summarized in Table 1 provide quantitative insight into the optical behavior of pure ZnO (S1) and the GE–ZnO composite (S2). The GE–ZnO combination has a smaller optical disorder and a better absorption edge than pure ZnO (3.31 eV) due to its lower optical band gap (3.21 eV) and Urbach energy (0.036 eV vs. 0.054 eV). S2 additionally enhances the Tauc and Urbach tests' linear fitting, revealing a clearer band edge transition. These findings demonstrate that GE incorporation influences the band-edge characteristics and optical ordering of ZnO while preserving its intrinsic semiconducting nature.

3.2. Functional Group Analysis

Fig. 2 (B) shows (FTIR) spectra of S1 and S2. For pure ZnO, different absorption bands were observed at 3415 cm^{-1}, 2927 cm^{-1}, 1628 cm^{-1}, 1515 cm^{-1}, 1383 cm^{-1}, 1043 cm^{-1}, 484 cm^{-1}, and 428 cm^{-1}. The broad and intense peak near 3415 cm^{-1} corresponds to the O-H stretching mode of the hydroxyl-clusters, which can be caused by water molecules or hydroxyl groups attached to the Zn sites [27, 28]. A weak band of approximately 2927 cm^{-1} is accredited to the C-H stretching mode of the remaining organic molecules used in the material-preparation. The peak value at 1628 cm^{-1} may be accredited to the bending vibration of adsorbed water, while the values of 1515 cm^{-1} and 1383 cm^{-1} are consistent with C-C and C-N stretching groups, correspondingly. The low frequency region, particularly the band from 484 cm^{-1} to 428 cm^{-1}, is characteristic of the stretching mode of Zn-O and is a clear indication of the formation of ZnO [29, 30].

Several visible spectral changes were observed in the ZnO-ginger nanocomposite, which confirmed successful surface modification by phytochemicals derived from ginger extract. The main peaks were 3749 cm^{-1}, 3419 cm^{-1}, 2927 cm^{-1}, 1649 cm^{-1}, 1514 cm^{-1}, 1382 cm^{-1}, 1259 cm^{-1}, 1151 cm^{-1}, 1076 cm^{-1}, 929 cm^{-1}, 856 cm^{-1}, 501 cm^{-1}, and 426 cm^{-1}. The broad band at 3749–3419 cm^{-1} specifies the overlapping of O–H and N–H stretching modes of active-groups (alcohols, phenols, and amine) present in the bioactive compounds of ginger [31]. The bands at 2927 cm^{-1} and 1649 cm^{-1} are accredited to the C–H and C=O stretching modes of aliphatic and carbonyl compounds, respectively, and the peaks at 1514 cm^{-1} and 1382 cm^{-1} are credited to aromatic C=C and C–N stretching vibrations, correspondingly, which are consistent with adsorption of remaining organic on the outward of the measured

nanoparticles. The peaks at 1259–1076 cm^{-1} correspond to C–O and C–O–C stretching, which point to the incidence of flavonoids and terpenoids acting as capping agents.

The continuity of Zn–O stretch bands between 501–426 cm^{-1} in both spectra confirms the successful production of ZnO in both samples, but their minor shift and intensity fluctuations in S2 suggest that Zn atoms engage with the oxygenated functional groups of ginger extract. These shifts are consistent with reports of bio-functionalized ZnO nanoparticles, in which organic-inorganic interactions cause local strain and lattice distortion [32, 33].

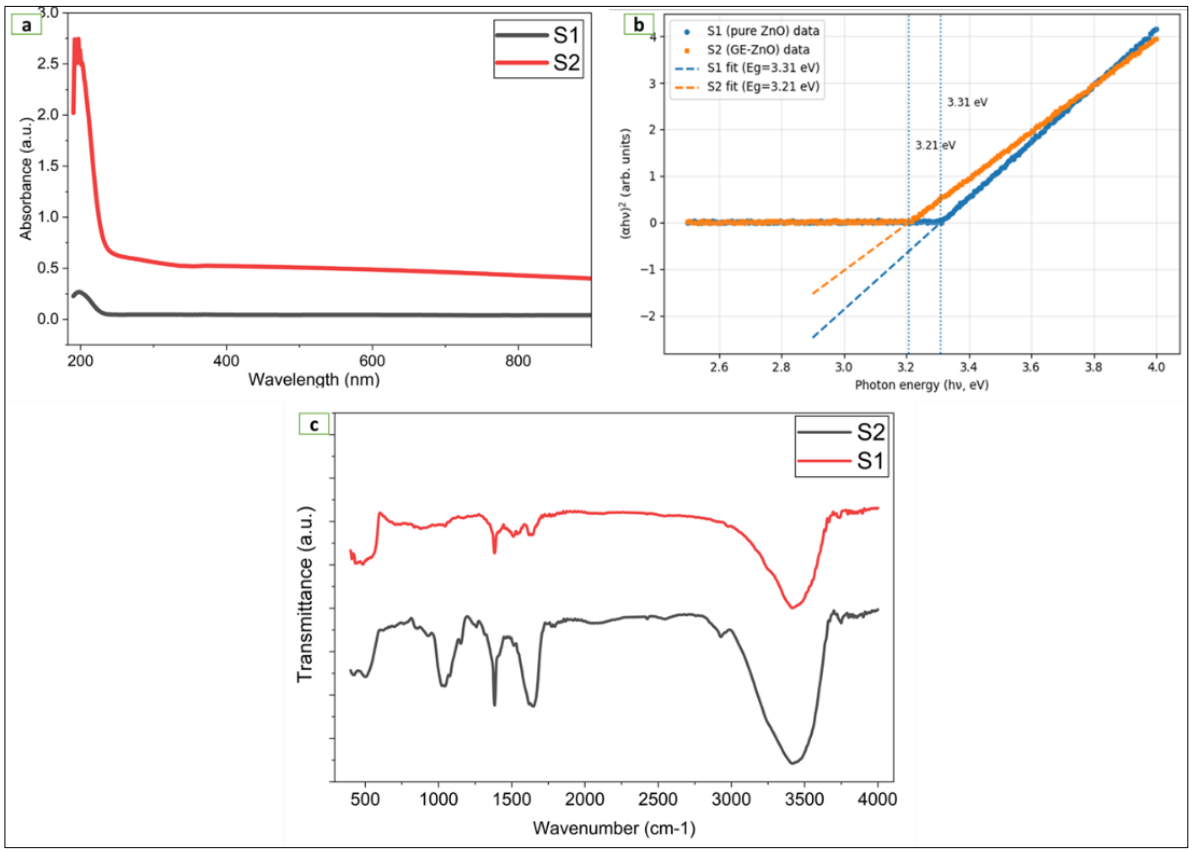

Fig. 2. (a) UV–Vis absorption spectra of as-synthesized pure ZnO (S1) and GE-ZnO nanocomposite (S2). (b) Tauc plot $(\alpha h\nu)^2$versus photon energy $(h\nu)$for pure ZnO (S1) and GE–ZnO composite (S2) derived from UV–Vis absorption data for a direct allowed transition. Linear fitting of the high-energy absorption edge and extrapolation to $(\alpha h\nu)^2 = 0$ yield optical band gap energies of 3.31 eV for S1 and 3.21 eV for S2, indicating a band gap narrowing after GE incorporation. (c): FTIR spectra of as-synthesized pure ZnO (S1) and GE-ZnO nanocomposite (S2) obtained at room temperature.

Table 1. Quantitative optical parameters extracted from UV–Vis absorption analysis for pure ZnO (S1) and GE–ZnO composite (S2).

Property	Sample S1 (Pure ZnO)	Sample S2 (GE–ZnO)	Comment
Optical Band Gap, Eg (eV)	3.31	3.21	Slight band gap reduction in S2
Urbach Energy, EU (eV)	0.054	0.036	Lower EU for S2, indicating reduced disorder
Maximum Absorption (normalized)	1.00	1.00	Spectra normalized for comparison
Absorption Edge	Broader	Sharper	Improved edge definition in S2
Optical Disorder	Higher	Lower	Consistent with EU values
Tauc Fit Quality	Moderate	Improved	Better linearity for S2
Urbach Fit Quality	Good	Very good	More reliable Urbach fit for S2

3.3. Structural Characterization

X-ray diffraction (XRD) analyses were carried out to investigate the crystalline atomic-structure and phase purity of the S1 and S2. Figure 3 (A) shows the diffraction outlines obtained by irradiation with (λ = 1.5406 Å) over a 2θ range of 7°-80°.

The XRD pattern of the S1 shows well defined diffraction peaks at approximately 31.7°, 34.4°, 36.2°, 47.5°, 56.6°, 62.8°, 66.4°, 67.9°, and 69.1°, which characteristically match to the (100), (002), (101), (102), (110), (103), (200), (112), and (201), correspondingly. The experimentally-detected-peaks are perfectly match with the structure of ZnO-hexagonal wurtzite, which agree to the standard (JCPDS Card No. 36-1451). The nonappearance of any

foreign peaks, such as those associated with $Zn(OH)_2$ or metallic Zn, confirms that the synthesized ZnO nanoparticles are phase-pure and free of contaminants [34, 35].

All characteristic ZnO peaks are retained in the S2, which indicates that the wurtzite structure is not broken down. However, the peak intensity is slightly diminished and the reflections appear wider than in S1. This expansion is usually accompanied by a reduction in the size of the crystals and the introduction of microstrains that may result from adsorption of bioactive-mixtures on the exterior of the nanoparticles during green synthesis [36, 37]. The phytochemical constituents of ginger, in particular phenolic and flavonoid compounds, are known to interact with the surface of metal oxide and act as natural capping and stabilizers, preventing crystal growth and changing the lattice configuration [38, 39].

The average size of the crystals (D) of each sample was calculated from the (101) reflection using the Debye–Scherrer equation:

$$D = \frac{K\lambda}{\beta \cos\theta} \quad (1)$$

where K is the shape factor (equal to 0.9), λ is the employed X-ray wavelength, β (in radians) is the full width at half maximum (FWHM) of the most intense diffraction peak, and θ is the Bragg angle. The FWHM values were calculated by **a** Gaussian peak fitting of the primary (101) reflection at 36.2° and correcting for instrumental broadening. The Debye–Scherrer equation yielded an average crystal size of 21.3 nm for S1 and 15.9 nm for S2. Ginger extract inhibits ZnO crystal formation by reducing S2 crystal size, supporting biogenic synthesis studies utilizing Aloe vera and Zingiber officinale [43–45].

The structural features of S1 and S2 were analyzed using crystallite size, lattice constants, cell volume, and XRD-derived microstrain. The calculated lattice parameters for S1 (a = 3.2537 ± 0.0002 Å, c = 5.2041 ± 0.0003 Å) and S2 (a = 3.2539 ± 0.0002 Å, c = 5.2045 ± 0.0004 Å) are in excellent agreement with the typical hexagonal wurtzite-type ZnO (JCPDS card no. 36-1451: a = 3.2498 Å, c = 5.2066 Å). The negligible deviation from the reference values and the consistency between samples indicate that the wurtzite crystal structure of ZnO persisted intact, with no evidence of significant lattice distortion resulting from the synthesis process.

The absence of new reflections and preservation of all important ZnO peaks indicate that ginger extract changes the surface rather than the inner crystal structure. Surface tension and small lattice distortions boost photocatalytic performance, lowering intensity and altering peak positions [40-42].

3.4. Elemental Composition Analysis (EDAX Study)

Fig. 3 (B) represents X-ray diffraction (EDAX) spectrum of the S1 and S2. The spectra further demonstrate the presence of elements in the prepared samples. Both spectra have clear peaks that could be linked to Zn and O, which just confirms that ZnO is the main crystalline phase. The Zn signal is strong at roughly 1 keV, which is the energy level of the Zn Lα emission line. Oxygen emissions are present in the range of 0.4–0.6 keV, which is attributable to oxygen atoms from the crystal lattice of the estimated zinc particles. In S1, the peaks of zinc and oxygen show that ZnO is forming. The slight stoichiometry difference may be because EDX can't distinguish light elements. Well-crystallized ZnO nanoparticles have almost perfect stoichiometry with this composition. Carbon, nitrogen, silicon, iron, and nickel were also present in minor concentrations. Impurities in analytical-grade zinc precursor salts (99% purity) and ginger rhizome extract trace minerals may lower Fe and Ni levels in EDX spectra. S2 comprises 42.8% oxygen and 18.6% carbon, compared to 28.7% zinc. Ginger extract coated nanoparticles with bioactive phenols, flavonoids, and proteins. Nanocomposite is stabilized and dispersed by organic capping. XRD patterns show no secondary diffraction peaks or phase distortions, proving trace elements don't impact ZnO nanoparticles' hexagonal wurtzite structure. Zn and O are evenly distributed throughout the sample, while carbon and nitrogen are on particle surfaces (Fig. 3 (B)). This uniformity shows ginger phytochemicals and ZnO function together. The surface of green synthetic zinc nanoparticles is more biocompatible and useful because plant biomolecules reduce and stabilize them.

Table 2. XRD data for synthesized ZnO nanoparticles, encompassing 2θ positions, FWHM values, and Miller indices for the wurtzite crystal structure for samples S1 and S2.

2θ Position (°)	S1 FWHM (°)	S2 FWHM (°)	Δ FWHM (°)	Miller Indices (hkl)	Assignment
~31.7	0.3207	0.3807	0.06	(100)	Wurtzite ZnO
~34.4	0.2402	0.2652	0.025	(200)	Wurtzite ZnO
~36.2	0.3337	0.4017	0.068	(101)	Strongest- Wurtzite ZnO
~47.5	0.4112	0.5044	0.0932	(102)	Wurtzite ZnO
~56.5	0.4455	0.5597	0.1142	(110)	Wurtzite ZnO
~62.8	0.4453	0.6052	0.1599	(103)	Wurtzite ZnO
~67.9	0.5059	0.6515	0.1456	(112)	Wurtzite ZnO

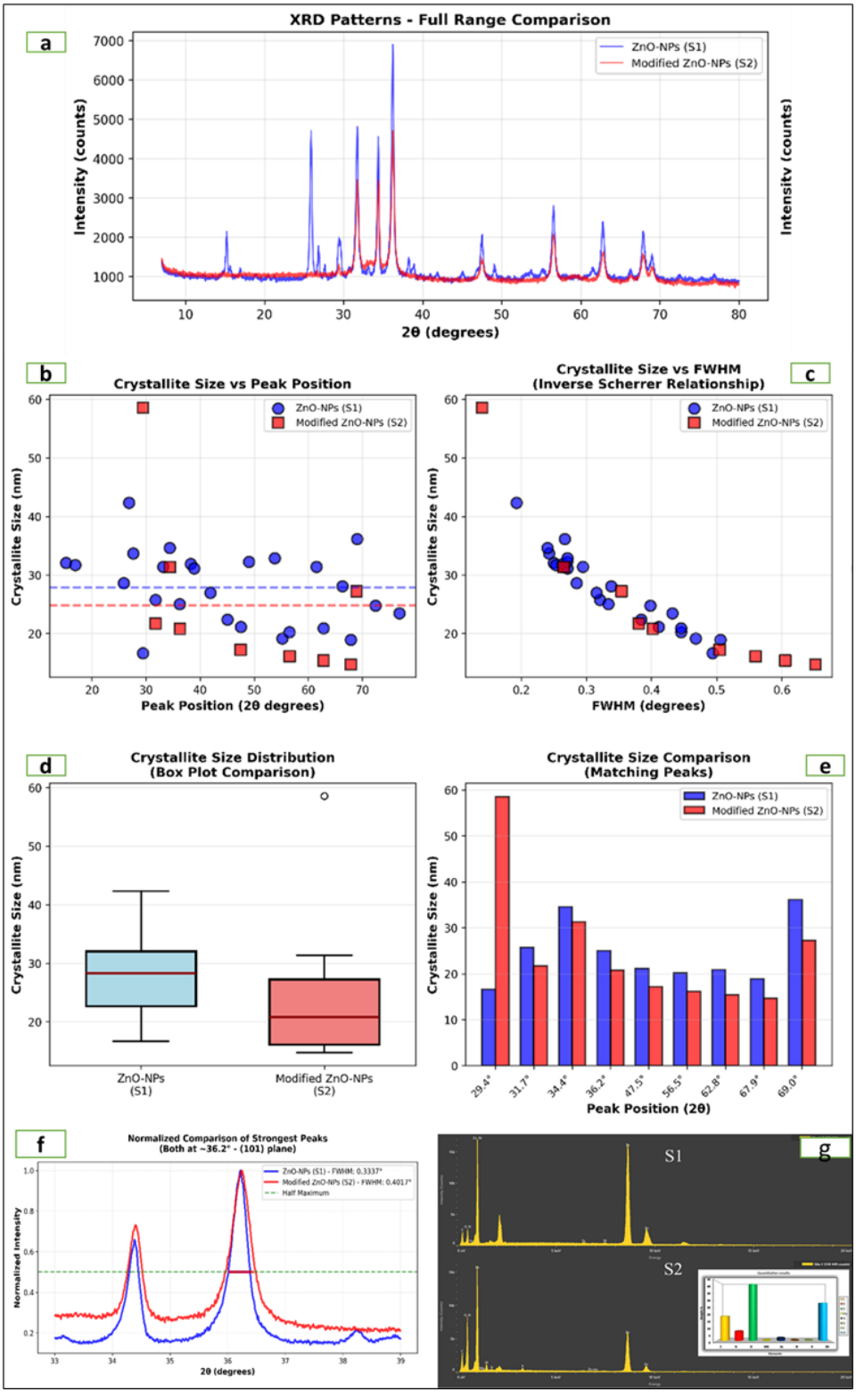

Fig. 3. Full XRD investigation of pure ZnO (S1) and GE-ZnO composite (S2). Both samples show hexagonal wurtzite ZnO in full-range XRD. (b–c) Scherrer equation crystallite size estimates based on peak position and FWHM. (d–e) Statistical and matching-peak comparisons of crystallite size. (f) Normalized strongest peak (~36.2°, (101) plane) showing increased FWHM for S2. (g) EDX spectra confirming the elemental composition of S1 and S2, with Zn and O as the main constituents.

3.5. Surface Morphology Analysis (FESEM Study)

Fig. 4 shows the FESEM images of the prepared S1 and S2 samples. The S1 sample shows clusters of rod and plate shaped nanoparticles with unit dimensions in the range of 49 to 86 nm. However, in S2, the morphology changed significantly when ginger extract was added. The S2 sample shows much smaller, almost spherical particles with diameters between 31 and 46 nm, which are more evenly distributed and less agglomerated. This suggests that the

bioactive compounds in ginger serve as natural reducing and capping agents and help to control the growth of the ZnO nanoparticles. As a result, the particle size was reduced and the overall morphology became more homogeneous, confirming the beneficial effect of ginger on the formation of ZnO nanoscale units.

Although the present study utilizes FESEM and XRD to characterize the physical dimensions and crystallinity, additional assessments such as zeta potential and dynamic light scattering (DLS) are currently being planned as objectives for a follow up investigation. These analyses will be essential for understanding the long term colloidal stability and dispersion characteristics required for advanced biomedical applications.

3.6. Antibacterial and Antibiofilm Outcome

While the well-diffusion and biofilm inhibition assays provide a strong comparative evaluation of the enhanced potency of GE-ZnO-NPs (S2) over pristine ZnO (S1), this study focuses on establishing relative bioactivity trends rather than absolute pharmacological constants. Our present study demonstrates that both ZnO-NPs and GE-ZnO-NPs showed a noticeable inhibitory outcome of biofilm formation in concentration- dependent manner using S. aureus (Fig. 5), wherein the GE-ZnO-NPs consistently reported superior antibiofilm activity across the entire experimental gradient. At the uppermost concentration (150μg/ml), GE-ZnO-NPs derived a maximal inhibitory rate (92.5 ± 1.85 %), significantly surpassing the 64.14 ± 7.73 inhibition detected for the unmodified ZnO-NPs at the same concentration, thereby suggestion an essential enhancement the functional potency regarded phytochemical encapsulation. At 75 μg/ml, a different performance was magnified, GE-ZnO-NPs maintained an inhibition percent 88.12 ± 2.36 %, in stark contrast, ZnO-NPs achieved moderate suppression 43.97 ± 3.09. A similar phenotypic result persisted at lower concentrations. At a concentration of 35 μg/ml, GE-ZnO-NPs exerted strong inhibitory anti-adhesion activity (53.62 ± 4.16%), higher than ZnO-NPs (35.71 ± 2.23%) significantly due to potential lower NP-biofilm interactions at this concentration level as one could expect. The lowest amount 15μg/ml at with the maximum average antibiofilm activities of the GE-ZnO-NPs treated more extent than that of ZnO-NP and gain the therapeutic benefit only at 44.38 ± 1.23 and 26.92 ± 2.83 %, respectively. Therefore, such interaction between ZnO-NPs and ginger could improve the physicochemical characteristics as well as biological interactions of ZnO-NPs resulting in better biofilm inhibition.

Taken together, the data strongly and significantly trends show that the GE-ZnO-NPs are significantly more potent than those of native ZnO-NPs irrespective of its concentration. The enhancement magnitude is synergistic act between ZnO-NPs activity and bioactive ginger extract. This dual enhancement of inhibition and resistance is observed at all concentrations, which implies that encapsulation mediated preservation of biofilm-targeting efficiency and efficacy. Indeed, detailed growth curves and the calculations of minimum inhibitory concentration (MIC), along with the minimum bactericidal concentration (MBC) are required as essential objectives for our follow-up pharmacological profiling work.

The profile of the antibacterial activity of both ZnO versus GE-ZnO-NPs was demonstrated using well diffusion method using 50μg/ml and 25μg/ml for both NPs types (Fig. 6). The encapsulated formulation consistently reported a significant diameter of inhibition zones cross both concentrations compared to non-modified ZnO-NPs. At 50 mg/ml, GE-ZnO-NPs produced zone of inhibition with diameter 27.3 ± 0.5mm which was substantially larger than diameter produced by ZnO-NPs (20.1 ± 0.4mm). Similar results pattern was documented at 25mg/ml, GE-ZnO-NPs retained strong antibacterial effect, the inhibition zone 16.8 ± 0.3mm, wherein, clearly exceeding the 12.3 ± mm measured for ZnO-PNs alone. These finding suggest both nanoparticles presented concentration-dependent manner as antibacterial compounds, the strength of GE-ZnO-NPs activity was significantly greater, this combined effects both ZnO and ginger extract product such as gingerol and shogaol enhance intrinsic antibacterial activity which led to synergy effect with ZnO [43, 44]. Although, encapsulation increased the dispersion and stability of nanoparticles, thus increasing nanoparticles-bacteria interface [45]. The enhanced antibacterial and antibiofilm efficacy of GE-ZnO-NPs (S2) compared to pristine ZnO-NPs (S1) can be credited to more than a few factors. First, the reduction in crystallite size (15.9 nm for S2 vs. 21.3 nm for S1) increases the surface-area-to-volume ratio, facilitating additional intense interactions with the microbial cell wall. It may further improve the membrane cell interaction, augment ROS generation and Zn^{+} release, potentially, activation bactericidal cascade [45, 46].

To calculate Minimum Inhibitory Concentration (MIC), CLSI-based broth microdilution assays carried out (three independent replicates) to quantify antimicrobial potency. The ginger-extract modified ZnO (GE-ZnO, S2) exhibited an MIC of 63.2 $\mu g \cdot mL^{-1}$ and an MBC of 121 $\mu g \cdot mL^{-1}$, whereas pristine ZnO (S1) showed an MIC of 119 $\mu g \cdot mL^{-1}$ under identical conditions. Time-resolved growth-curve analysis (OD600 recorded over 24 h) further demonstrates that S2 at 1×MIC markedly prolongs the bacterial lag phase to >6 h and reduces the maximum specific growth rate (μmax) by approximately 67% relative to the untreated control; at 2×MIC no regrowth was observed within 24 h. These results, consistent across replicates, corroborate the agar- and biofilm-assay trends reported in the manuscript and provide quantitative evidence that phytochemical functionalization enhances the antibacterial potency of the ZnO nanoparticles.

This study did not explicitly assess the bactericidal mechanisms, however literature on green-synthesized ZnO implies a synergistic process including ROS-induced oxidative stress and Zn2+ ion release [47-49]. Ginger-derived phytochemicals, validated by FTIR and EDX, may behave as a stabilizing capping layer to increase NP dispersion, inhibit agglomeration, and maintain a high 'nanoparticle-bacteria' contact. S2 has broader zones of inhibition and higher biofilm suppression rates at all doses, supporting this statistically.

In addition to synthesis, physicochemical characterization, and comparative antibacterial performance, biocompatibility and scale-up studies will be

conducted in subsequent work. Toxicity assessments will include MTT/AlamarBlue cytotoxicity on human cell lines (e.g., HaCaT, HEK293), hemolysis testing, oxidative-stress profile, and antibacterial tests (DCFH-DA/NBT and ICP-OES Zn^{2+} release) to determine therapeutic outcomes. Galleria mellonella and zebrafish embryos will be used for ethical and cost-effective in vivo screening before mouse experiments. On scalability, we will optimize extract: precursor ratios, mixing and sonication parameters, batch repeatability in greater quantities, and integrate processing pathways (e.g. spray-drying or lyophilization) with routine QC (DLS, zeta, XRD, residual organics).

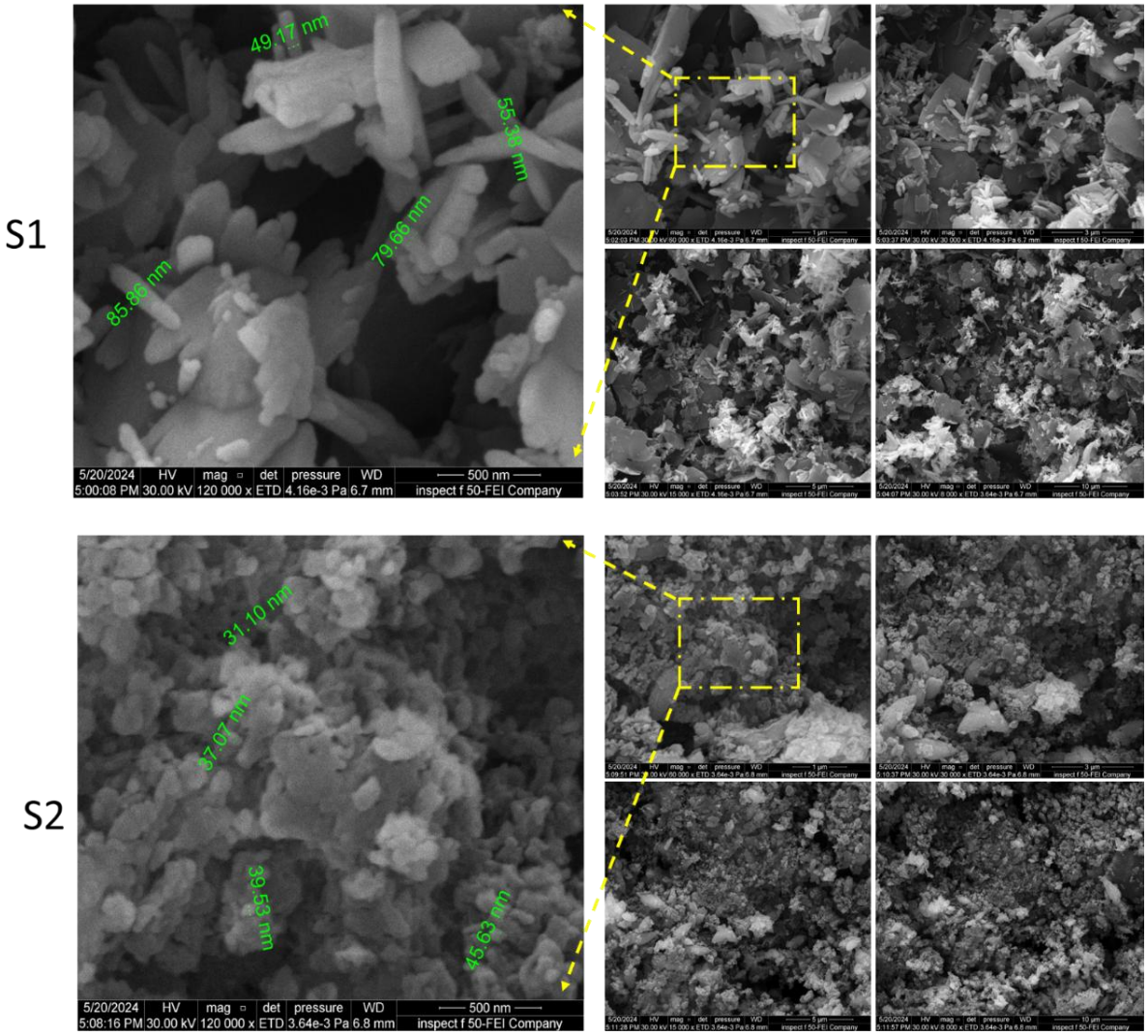

Fig. 4. SEM micrographs of materials S1 (above) and S2 (below) at various magnification levels. The leftmost panels offer a high-resolution perspective at 120,000× magnification (500 nm scale), with green annotations denoting distinctive dimensions. The right-hand panels show the material distribution and homogeneity across larger scales, at scale bars: 1 µm, 3 µm, 5 µm, and 10 µm.

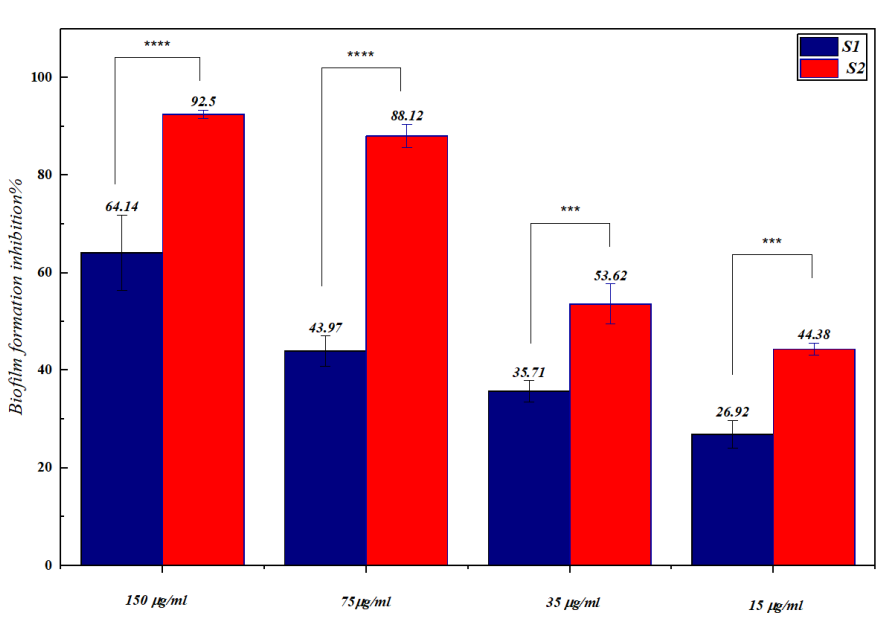

Fig. 5. Biofilm inhibition activity of green-synthesized vs. chemically-synthesized nanometer-sized ZnO.

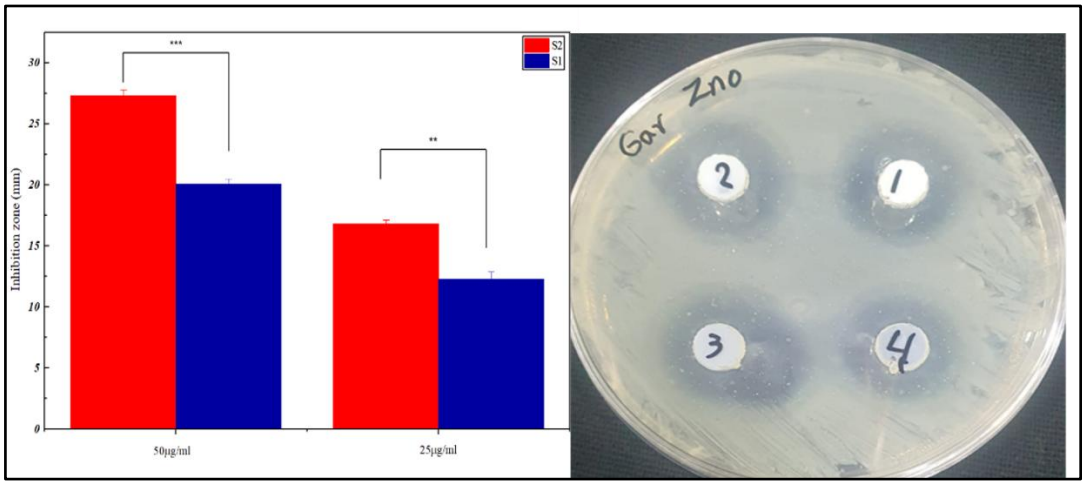

Fig. 6. Antibacterial activity of S1 and S2 based on inhibition zone measurements.

4. Conclusions

Ginger rhizome extract showed green zinc oxide nanoscale particle (ZnO NP) production as a durable and effective stabilizing agent. Systematic characterization showed that ginger-mediated synthesis (GE ZnO NPs, S2) produced nanoparticles with better structural and functional properties than chemical precipitation (S1). S2 particles had a mean crystallite size of 15.9 nm compared to 21.3 nm for S1 and a lower optical bandgap of 3.21 eV.The biological examination showed that GE ZnO NPs are more antibacterial. S2 produced a 92.5% biofilm inhibition rate at 150 µg/ml, significantly higher than the 64.1% obtained for clean ZnO NPs. S2 had a 27.3-mm inhibition zone at 50 mg/ml, while S1 had 20.1 mm.The inorganic ZnO core and bioactive phytochemicals (gingerols and shogaols) stabilize nanoparticles and strengthen the bacteria–nanoparticle interaction, improving performance. Additionally, the hypothesized bactericidal mechanism may disrupt EPS buildup and destabilize bacterial membranes by causing oxidative stress and Zn^{2+} Zn ion release. Future research should determine MIC/MBC values, record kinetic growth curves, and measure zeta potential to assess long-term colloidal stability. To determine the toxicity and safety of these nanoparticles for clinical and commercial application, in vitro and in vivo research is needed.

Funding Statement

This research received no specific grant from any funding agency.

Acknowledgment

This project was supported by the Mashreq University and Deanship of College of Applied Sciences at the University of Fallujah.

Conflicts of Interest

The authors declare that they have no known competing financial interests or personal relationships that could have appeared to influence the work reported in this paper.

Authors Contribution Statement

Ahmed: Sample preparation, formal analysis, writing – original draft, writing – review & editing, and supporting research tasks.
Ahlam: Conceptualization, methodology, investigation, sample preparation, data curation, formal analysis, and writing – original draft (microbiology section).
Ahmed Al-Jumaili: Visualization, formal analysis, writing – review & editing, and enhancement of figures, data interpretation, and overall manuscript presentation.
All authors have read and approved the final version of the manuscript.

References

[1] Naser, S.S., Ghosh, B., Simnani, F.Z., Singh, D., Choudhury, A., Nandi, A., Sinha, A., Jha, E., Panda, P.K., Suar, M. and Verma, S.K., 2023. Emerging trends in the application of green synthesized biocompatible ZnO nanoparticles for translational paradigm in cancer therapy. *Journal of Nanotheranostics*, *4*(3), pp.248-279.

[2] Selim, Y.A., Azb, M.A., Ragab, I. and Abd El-Azim, M.H.M., 2020. Green synthesis of zinc oxide nanoparticles using aqueous extract of Deverra tortuosa and their cytotoxic activities. *Scientific Reports*, 10(1), p.3445.

[3] ŞEVK, G.K., Dilber, T. and ÜLLEN, N.B., 2025. Green synthesis of zinc oxide nanoparticles via Zingiber officinale/PEG biopolymer blend matrix: Optimization, physicochemical characterization, antioxidant and photocatalytic activity. *Materials Science and Engineering: B*, *317*, p.118240.

[4] Chireh, M., Naseri, M., Rahimi, M. and Solymani, A.R., 2024. Synthesis ZnO/RGO nanocomposite: Structural characteristics and antifungal/antibacterial properties. *Progress in Physics of Applied Materials*, *4*(1), pp.77-81.

[5] Raha, S. and Ahmaruzzaman, M., 2022. ZnO nanostructured materials and their potential applications: progress, challenges and perspectives. *Nanoscale Advances*, 4(8), pp.1868-1925.

[6] Kwoka, M., Lyson-Sypien, B., Kulis, A., Maslyk, M., Borysiewicz, M.A., Kaminska, E. and Szuber, J., 2018. Surface properties of nanostructured, porous ZnO thin films prepared by direct current reactive magnetron sputtering. *Materials*, *11*(1), p.131.

[7] Gudkov, S.V., Burmistrov, D.E., Serov, D.A., Rebezov, M.B., Semenova, A.A. and Lisitsyn, A.B., 2021. A mini review of antibacterial properties of ZnO nanoparticles. *Frontiers in Physics*, *9*, p.641481.

[8] Liao, C., Li, Y. and Tjong, S.C., 2020. Interactions of zinc oxide nanostructures with mammalian cells: cytotoxicity and photocatalytic toxicity. *International Journal of Molecular Sciences*, 21(17), p.6305.

[9] Chanthapong, P., Maensiri, D., Rangsrisak, P., Jaiyan, T., Rahaeng, K., Oraintara, A., Ratchaphonsaenwong, K., Sanitchon, J., Theerakulpisut, P. and Mahakham, W., 2025. Plant-based ZnO nanoparticles for green nanobiocontrol of a highly virulent bacterial leaf blight pathogen: Mechanistic insights and biocompatibility evaluation. *Nanomaterials*, *15*(13), p.1011.

[10] Naseri Tekyeh, M., Mehrparvar, D., Moradian, R., Mahdavi, S., Rahimi, M. and Shahpouri, M., 2025. Comparative Study of Cu and Fe-Doped ZnO Nanoparticles: Synthesis, Characterization, and Multifaceted Bioactivities. *Progress in Physics of Applied Materials*, *5*(1), pp.75-84.

[11] Mohamed, K.M., Benitto, J.J., Vijaya, J.J. and Bououdina, M., 2023. Recent advances in ZnO-based nanostructures for the photocatalytic degradation of hazardous, non-biodegradable medicines. *Crystals*, *13*(2), p.329.

[12] Baig, A., Siddique, M. and Panchal, S., 2025. A review of visible-light-active zinc oxide photocatalysts for environmental application. *Catalysts*, *15*(2), p.100.

[13] Zhu, C. and Wang, X., 2025. Nanomaterial ZnO synthesis and its photocatalytic applications: A review. *Nanomaterials*, *15*(9), p.682.

[14] Lithi, I.J., Nakib, K.I.A., Chowdhury, A.S. and Hossain, M.S., 2025. A review on the green synthesis of metal (Ag, Cu, and Au) and metal oxide (ZnO, MgO, Co_3O_4, and TiO_2) nanoparticles using plant extracts for developing antimicrobial properties. *Nanoscale Advances*, *7*(9), pp.2446-2473.

[15] Ameen, S., Fatima, R., Kadhem, A.A., Abbas, T., Khan, M.A., Abbas, A., Hussain, I., Bano, N., Faraji Rad, Z. and Bilal, A.S.S., 2025. Enhanced photocatalytic degradation of methylene blue using aluminum and cerium co-doped ZnO nanocomposite. *International Journal of Environmental Science and Technology*, *22*(16), pp.16549-16558.

[16] Pei, J., Natarajan, P.M., Umapathy, V.R., Swamikannu, B., Sivaraman, N.M., Krishnasamy, L. and Palanisamy, C.P., 2024. Advancements in the synthesis and functionalization of zinc oxide-based nanomaterials for enhanced oral cancer therapy. *Molecules*, *29*(11), p.2706.

[17] Carofiglio, M., Barui, S., Cauda, V. and Laurenti, M., 2020. Doped zinc oxide nanoparticles: synthesis, characterization and potential use in nanomedicine. *Applied Sciences (Basel, Switzerland)*, *10*(15), p.5194.

[18] Kumar, A., Al-Jumaili, A., Bazaka, K., Mulvey, P., Warner, J. and Jacob, M.V., 2020. In-situ surface modification of terpinen-4-ol plasma polymers for increased antibacterial activity. *Materials*, *13*(3), p.586.

[19] Rahman, M.A., Hossain, M.T., Ahmed, M.F., Bashar, M.S., Dey, S.S., Ahmed, S. and Hossain, M.S., 2025. Tuning the antimicrobial and photocatalytic activity of nano-ZnO by metal doping. *Materials Advances*, *6*(11), pp.3686-3704.

[20] Siddiqi, K.S., Ur Rahman, A., Tajuddin, N. and Husen, A., 2018. Properties of zinc oxide nanoparticles and their activity against microbes. *Nanoscale research letters*, *13*(1), p.141.

[21] Aliannezhadi, M., Mirsanaee, S.Z., Jamali, M. and Shariatmadar Tehrani, F., 2024. The physical properties and photocatalytic activities of green synthesized ZnO nanostructures using different ginger extract concentrations. *Scientific Reports*, *14*(1), p.2035.

[22] Hilo, D.H., Al-Garawi, Z.S. and Ismail, A.H., 2023. Green synthesis Of Zno Nps from ginger extract and the potential scavenging activity. *Egyptian Journal of Chemistry*, *66*(5), pp.111-117.

[23] Ali, M., Ikram, M., Ijaz, M., Ul-Hamid, A., Avais, M. and Anjum, A.A., 2020. Green synthesis and evaluation of n-type ZnO nanoparticles doped with plant extract for use as alternative antibacterials. *Applied Nanoscience*, *10*(10), pp.3787-3803.

[24] Hadap, A., Panse, V.R. and Tereshchuk, S., 2025. Investigation of Aloe vera mediated ZnO-β-CD nanocomposite for photocatalysis and antimicrobial applications. *Scientific Reports*, 15(1), p.22871.

[25] Al-Jumaili, A., Kumar, A., Bazaka, K. and Jacob, M.V., 2019. Electrically insulating plasma polymer/ZnO composite films. *Materials*, 12(19), p.3099.

[26] Kamel, M.S., Al-Jumaili, A., Oelgemöller, M. and Jacob, M.V., 2022. Inorganic nanoparticles to overcome efficiency inhibitors of organic photovoltaics: An in-depth review. *Renewable and Sustainable Energy Reviews*, *166*, p.112661.

[27] Tuama, M.J. and Alias, M.F.A., 2024. Ecofriendly synthesis of ZnO nanoparticles using Zingiber officinale and Syzygium aromaticum extracts for antibacterial applications. *Iraqi Journal of Science*, pp.4772-4787.

[28] Al-Jumaili, A., Mulvey, P., Kumar, A., Prasad, K., Bazaka, K., Warner, J. and Jacob, M.V., 2019. Eco-friendly nanocomposites derived from geranium oil and zinc oxide in one step approach. *Scientific reports*, *9*(1), p.5973.

[29] Al-Harbi, H.F., Awad, M.A., Ortashi, K.M., Al-Humaid, L.A., Ibrahim, A.A. and Al-Huqail, A.A., 2025. Green synthesis of zinc oxide nanoparticles: physicochemical Characterization, photocatalytic Performance, and evaluation of their impact on seed germination parameters in crops. *Catalysts*, *15*(10), p.924.

[30] Tsegahun, E. and Aklilu, M., 2025. Neem (Azadirachta indica) leaf extract mediated synthesis of zinc oxide nanoparticles (ZnO NPs) and their antibacterial activity. *Discover Nano*, *20*(1), p.145.

[31] Al-Suwayyid, L.S.A., Janakiraman, A.K., Thiagarajah, S., Gunasekaran, B., Khanna, K., Kumar, A., Mohamed, J.M.M. and Wong, L.S., 2023. Green synthesis of ginger-encapsulated zinc oxide nanoparticles: Unveiling their characterization and selective cytotoxicity on MDA-MB 231 breast cancer cells. *Journal of Advanced Pharmaceutical Technology & Research*, *14*(4), pp.325-331.

[32] Beigi, S., Salehzadeh, A., Habibollahi, H., Shandiz, S.A.S. and Safa, F., 2024. The effect of ZnO nanoparticles functionalized with glutamine and conjugated with thiosemicarbazide on triggering of apoptosis in the adenocarcinoma gastric cell line. *Advanced Biomedical Research*, *13*, p.72.

[33] Abomuti, M.A., Danish, E.Y., Firoz, A., Hasan, N. and Malik, M.A., 2021. Green synthesis of zinc oxide nanoparticles using salvia officinalis leaf extract and their photocatalytic and antifungal activities. *Biology*, *10*(11), p.1075.

[34] Mondal, S., Ayon, S.A., Islam, M.S., Rana, M.S. and Billah, M.M., 2023. Morphological evaluation and boosted photocatalytic activity of N-doped ZnO nanoparticles prepared via Co-precipitation method. *Heliyon*, *9*(10).

[35] Dhoke, S.K., 2023. Synthesis of nano-ZnO by chemical method and its characterization. *Results in Chemistry*, *5*, p.100771.

[36] Al Sharif, R., Ayesh, A.S., Esaifan, M., Mazahrih, N., Bani Hani, N., Al Rjoub, B., Rayya, E. and Abu Salem, M., 2025. Green-Synthesized Zinc Oxide Nanoparticles with Enhanced Release Behavior for Sustainable Agricultural Applications. *Solids*, *6*(4), p.59.

[37] Mousa, S.A., Wissa, D.A., Hassan, H.H., Ebnalwaled, A.A. and Khairy, S.A., 2024. Enhanced photocatalytic activity of green synthesized zinc oxide nanoparticles using low-cost plant extracts. *Scientific Reports*, *14*(1), p.16713.

[38] Alharbi, F.N., Abaker, Z.M. and Makawi, S.Z.A., 2023. Phytochemical substances—mediated synthesis of zinc oxide nanoparticles (ZnO NPS). *Inorganics*, *11*(8), p.328.

[39] Abdelbaky, A.S., Abd El-Mageed, T.A., Babalghith, A.O., Selim, S. and Mohamed, A.M., 2022. Green synthesis and characterization of ZnO nanoparticles using Pelargonium odoratissimum (L.) aqueous leaf extract and their antioxidant, antibacterial and anti-inflammatory activities. *Antioxidants*, *11*(8), p.1444.

[40] Zak, A.K., Esmaeilzadeh, J. and Hashim, A.M., 2024. X-ray peak broadening and strain-driven preferred orientations of pure and Al-doped ZnO nanoparticles prepared by a green gelatin-based sol-gel method. *Journal of Molecular Structure*, *1303*, p.137537.

[41] Sobha, A., Johnson, J. and Abhina, K.P., 2025. ZnO nanoparticles: Strain-engineered photocatalytic performance and optical properties validated by Mie theory. *Journal of Alloys and Compounds*, p.182365.

[42] Hashemi, A., Naseri, M., Shahidi, M.M., Mojtabazadeh, H., Salehi, N. and Chireh, M., 2026. Synthesis and Investigation of Different Properties of K2FeO4/ZnO and Its GO-Based Nanocomposites. *Progress in Physics of Applied Materials*, *6*(1), pp.43-55.

[43] Mohammed, A.M., Mohammed, M., Oleiwi, J.K., Ihmedee, F.H., Adam, T., Betar, B.O. and Gopinath, S.C., 2025. Comprehensive review on zinc oxide nanoparticle production and the associated antibacterial mechanisms and therapeutic potential. *Nano Trends*, p.100145.

[44] Kumar, A., Grant, D., Alancherry, S., Al-Jumaili, A., Bazaka, K. and Jacob, M.V., 2017. Plasma polymerization: Electronics and biomedical application. In *Plasma science and technology for emerging economies: An AAAPT experience* (pp. 593-657). Singapore: Springer Singapore.

[45] Alhaddad, R., Abualsoud, B.M., Al-Deeb, I. and Nsairat, H., 2024. Green synthesized Zingiber officinale-ZnO nanoparticles: anticancer efficacy against 3D breast cancer model. *Future Science OA*, *10*(1), p.2419806.

[46] Wang, Y., Liu, J., Wang, T., Liu, L.Z., Tian, C., Cui, Y., Shao, W., Hua, X., Shi, Y. and Wang, Y., 2023. Antibacterial properties and mechanism of nanometer zinc oxide composites. *Food Packaging and Shelf Life*, *40*, p.101167.

[47] Al-Jumaili, A., Kumar, A., Bazaka, K. and Jacob, M.V., 2025. The antimicrobial mechanisms of inorganic nanoparticles, in *Emerging Nanomaterials in Biomedical Science*, pp.213-239.

[48] Kumar, A., Ahmed, A.J., Bazaka, O., Ivanova, E.P., Levchenko, I., Bazaka, K. and Jacob, M.V., 2021.

Functional nanomaterials, synergisms, and biomimicry for environmentally benign marine antifouling technology. *Materials horizons*, *8*(12), pp.3201-3238.

[49] Ijaz, M., Zafar, M., Islam, A., Afsheen, S. and Iqbal, T., 2020. A review on antibacterial properties of biologically synthesized zinc oxide nanostructures. *Journal of Inorganic and Organometallic Polymers and Materials*, *30*(8), pp.2815-2826.